

A PLAN FOR THE DEVELOPMENT OF SUPERCONDUCTING UNDULATOR PROTOTYPES FOR LCLS-II AND FUTURE FELS

P. Emma, N. Holtkamp, H.-D. Nuhn, SLAC, Stanford, CA 94309, USA

D. Arbelaez, J. Corlett, S. Myers, S. Prestemon, R. Schlueter, LBNL, Berkeley, CA 94720, USA

C. Doose, J. Fuerst, Q. Hasse, Y. Ivanyushenkov, M. Kasa, G. Pile, E. Trakhtenberg, E. Gluskin, ANL, Argonne, IL 60439, USA

Abstract

Undulators serve as the primary source of radiation for modern storage rings, and more recently for the advent of Free-Electron Lasers (FELs). The performance of future FELs can be greatly enhanced using the much higher magnetic fields of superconducting undulators (SCU) [1]. For example, the LCLS-II hard x-ray undulator can be shortened by up to 70 m using an SCU in place of a PMU (permanent magnet undulator), or its spectral performance can be critically improved when using a similar length. In addition, SCUs are expected to be orders of magnitude less sensitive to radiation dose; a major issue at LCLS-II with its 1-MHz electron bunch rate. We present a funded R&D collaboration between SLAC, ANL, and LBNL, which aims to demonstrate the viability of superconducting undulators for FELs by building, testing, measuring, and tuning two 1.5-m long planar SCU prototypes using two different technologies: *NbTi* at ANL and *Nb₃Sn* at LBNL. Our goal is to review and reassess the LCLS-II HXR baseline plans (PMU) in July of 2015, after the development and evaluation of both prototypes, possibly in favor of an SCU for LCLS-II.

INTRODUCTION

The LCLS-II [2] FEL project at SLAC aims to construct a new continuous wave (CW), 4-GeV superconducting linac (SC-linac) [3], to feed either of two new undulators: 1) the Soft X-ray Undulator (SXU), or 2) the Hard X-ray Undulator (HXU). The HXU replaces the existing LCLS-I fixed-gap undulator and can be optionally fed by the existing 3-15-GeV copper (Cu) linac (120 Hz), presently used to drive the LCLS-I FEL. The spectral requirements for the SXU are 0.2-1.3 keV (SASE and self-seeded), while the HXU requires 1 keV to ≥ 5 keV (SASE, and self-seeded where possible) when driven by the SC-linac. The HXU spectral range, when driven by the Cu-linac (3-15 GeV), requires 1-25 keV.

The present (2014) baseline design uses two adjustable-gap, planar PMUs (NdFeB) with 39-mm (SXU) and 26-mm (HXU) periods and a 7.2-mm full magnetic gap, g_m . At 4 GeV (limited by SC-linac costs) the PMUs reach these requirements, but with little margin, especially in the HXU which barely produces 5 keV SASE, and cannot exceed 4 keV when self-seeded (limited hall length).

To remove these performance limitations, we propose an SCU undulator, at least for the HXU system, which significantly extends the spectral range when driven by the SC-linac, outperforms the presently foreseen PMU, and can even provide > 1 TW peak power when self-

seeded, tapered, and driven by the Cu-linac. It also offers much less magnetic field sensitivity to radiation dose, an issue greatly magnified by the high-rate, high power linac.

Unresolved technical risk issues for SCU systems, such as field correction, and limited experience with SCUs in operating machines [4], [5], have led to an R&D plan with a goal of building, testing, and correcting two 1.5-m long prototype FEL undulators by July 2015 which meet LCLS-II HXU specifications using two different conductors: *NbTi* (21 mm period), and *Nb₃Sn* (19 mm period), each with an 8-mm magnet gap.

FEL PERFORMANCE MOTIVATION

The motivations for SCUs, especially in comparison to PMUs (“in” or “out” of vacuum), are listed below.

- Higher magnetic fields allow superior FEL performance, or reduced undulator length.
- No permanent magnetic material to be damaged by radiation, allowing long life and smaller gaps.
- Reduced resistive wakefield with a cold bore? [6].
- Much lower vacuum pressure limits gas scattering.
- Smaller footprint and simpler *K*-control than the typical massive adjustable-gap PMU.
- Easily oriented for vertical polarization, if desired.

Figure 1 shows LCLS-II (HXU, SC-linac) calculations [7] of the full undulator system length (2-m magnet segments and 0.7-m breaks; each with a BPM, quadrupole, and phase shifter) versus the upper-limit SASE photon energy that saturates within 80% of that undulator length at 4 GeV (beam parameters in Table 1).

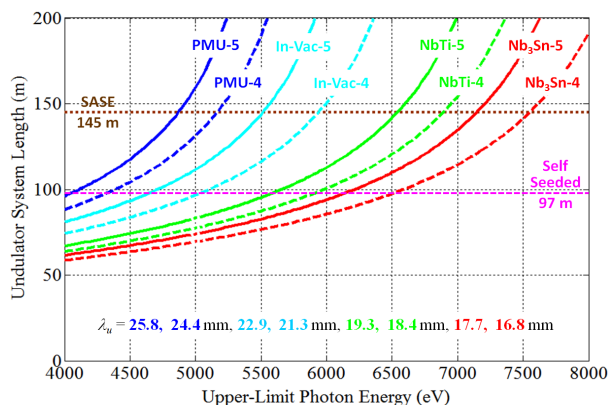


Figure 1: Undulator system length (with breaks) versus upper-limit SASE photon energy saturating in 80% of that undulator length at 4 GeV. Existing 145-m und. hall length is indicated.

The lower-limit photon energy is chosen at 1.5 keV for all curves (at 4 GeV), so once the magnet gap and undulator technology (e.g., NdFeB-PMU, NbTi-SCU, or Nb₃Sn-SCU) are chosen, the period is then exactly given from the FEL resonance condition,

$$\lambda_r = \frac{\lambda_u}{2\gamma^2} (1 + K^2/2),$$

where λ_r is the FEL wavelength, λ_u is the period, γ is the electron energy in units of rest mass, and K is the undulator parameter ($K \approx 0.93 \cdot B_{pk}[\text{T}] \lambda_u[\text{cm}]$), where the peak field, B_{pk} , is a known function of the magnet gap, g_m , period, and the precise undulator technology used.

All “5” labels (e.g., “PMU-5”) in Figure 1 have 5-mm vacuum gaps (7.3-mm magnet gaps), while “4” labels (e.g., “PMU-4”) are 1-mm smaller. The “in-vacuum” is the same PMU technology and has the same (4-mm and 5-mm) vacuum gaps for fair comparison, but 2-mm smaller magnet gaps. Periods are shown for all 8 cases.

The SCU performance is superior to the PMU (both “in-vac” and “out-of-vac”) allowing up to 7.6 keV SASE saturation in a 145-m undulator (whereas LCLS-II baseline design allows just 5 keV). Clearly the “in-vacuum” performs better than the “out-of-vacuum”, but neither reaches the attractive performance levels of the SCUs. The Nb₃Sn promises the best performance, but involves more risk with a 650°C heat treatment cycle required. Note that self-seeding requires 50% more undulator, so the highest self-seeded photon energy is the intersection of these curves with the 97-m line (e.g., 6.5 keV for Nb₃Sn-4). The parameters used in these calculations (and TW discussion below) are in Table 1.

Table 1: Parameters used for FEL Calculations (SC & Cu-linac)

Parameter	Sym.	SC-linac	Cu-linac	unit
Electron energy	E_0	4.0	6.6	GeV
Emittance	$\gamma \epsilon_{x,y}$	0.4	0.4	μm
Energy spread, rms	σ_E	0.5	1.5	MeV
Peak current	I_{pk}	1	4	kA
Und. period	λ_u	16.8	16.8	mm
Und. magnet gap	g_m	6.3	6.3	mm
Und. vacuum gap	g_v	4.0	4.0	mm

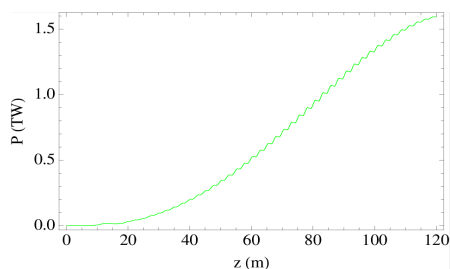


Figure 2: Peak power (1.6 TW) at 4 keV using same “Nb₃Sn-4” undulator of Figure 1, but now self-seeded, tapered, and driven by the Cu-linac at 6.6 GeV with 4 kA (see Table 1). Segment lengths are 2 m long, which is optimal for this 1-m gain length.

In addition to this spectral range extension, when the same “Nb₃Sn-4” undulator (or similar for “NbTi-4”) is driven by the Cu-linac at 6.6 GeV (120 Hz), with self-seeding [8], and a step-wise field taper applied to each 2-m undulator segment (20% total taper), a peak FEL power of 1.6 TW at 4 keV is possible (see Figure 2 and Table 1). Here the self-seeding monochromator is at $z = 0$.

SCU R&D PLAN

The goal of this R&D effort is to demonstrate the viability of SCU technology for FEL undulators by building, measuring, testing, and correcting two prototype SCUs. The parameters, such as magnetic field strength for the chosen period and gap, and field quality over the undulator length, must be demonstrated. The parameter selection is dictated by the desired spectral range of x-rays and the electron energy of LCLS-II. As a result, with an 8-mm prototype gap, the undulator period lies between 19 and 21 mm, depending on the superconductor. The vacuum gap is 5.7 mm. The undulator segment length should not be too long, in order to avoid practical difficulties, and is chosen as 1.5 m for the prototype, representing a reasonable building block for a long undulator line. This length also conveniently fits the existing 2-m long test cryostat at ANL [4] for prototype testing. A full-scale SCU system may use a longer segment and smaller gap, but this needs more study.

We will build two 1.5-m long superconducting planar undulator magnetic structures, one from NbTi (ANL) and another from Nb₃Sn (LBNL), with independent cryogenic testing on each using the same (existing) APS 2-m cryostat, verifying the magnetic performance of each undulator using the same magnet measurement bench. It will also employ a unique magnetic tuning approach developed at LBNL [9] (see below). The project design and execution relies heavily on well-established designs of the cryostat, undulator magnet core, and magnetic measurement systems developed and implemented for shorter undulators at the APS [10].

The APS SCU magnetic measurement system incorporates Hall-probe and rotating coil sensors modified for the smaller vacuum pipe diameter. The system will also incorporate a pulsed-wire technique developed at LBNL [11]. The project deliverable will be two fully functional superconducting undulators that meet LCLS-II undulator specifications by July 2015. Prototype undulator parameters are listed in Table 2, showing the slightly different period for each magnet.

Table 2: SCU Prototype Parameters

Parameter	Symbol	NbTi	Nb ₃ Sn	Unit
Magnetic full gap	g_m	8	8	mm
Vacuum chamber gap	g_v	5.7	5.7	mm
Und. period	λ_u	21	19	mm
Magnet length	L_m	1.5	1.5	m
Peak magnetic field	B_{pk}	1.66	1.86	T
Max. K value	K_{max}	3.27	3.31	-

PROTOTYPE MAGNET DESIGNS

Two 1.5-m long magnets are being developed, with NbTi conductor at ANL and Nb₃Sn at LBNL, each based on recent SCU development experience [4], [12]. The magnet designs are described for each technology below.

The Niobium-Titanium Magnet (NbTi)

The NbTi magnet is a scaled up version of the 1.1-m long SCU1 magnet, the second superconducting undulator currently being built at the Advanced Photon Source (APS) of ANL. The magnetic design is similar to that of SCU0 [13], the first SCU currently in operation at the APS. It consists of a pair of identical magnets, or jaws, separated by a gap where a beam chamber is accommodated. Each jaw is a series of vertical racetrack superconducting coil packs (53 turns) wound with a round 0.7-mm wire, and separated by magnetic poles, with currents flowing in opposite directions in adjacent coil packs. The winding form is made of low carbon steel to increase the undulator peak field. Each jaw has a main coil and there are two pairs of correction coils that are wound on top of the main coil in the first and last two end grooves. The correction coils are separately powered and are used mainly for tuning the second field integral since the first integral is automatically zeroed due to a chosen asymmetric magnetic configuration.

The design model of the magnet is shown in Figure 3. The superconducting coils are indirectly cooled by liquid helium passing through the channels in the cores; the flanges of the *LHe* circuit are visible in the Figure.

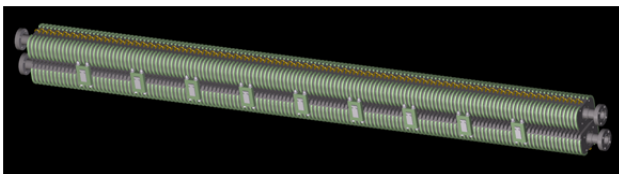


Figure 3: NbTi prototype undulator magnet design.

The Niobium-3-Tin Magnet (Nb₃Sn)

A prototype using Nb₃Sn superconductor is being fabricated at LBNL. The high transport current provided by Nb₃Sn conductors is leveraged in order to attain the highest possible magnetic field in the undulator. Nb₃Sn is an intermetallic compound with an A15 lattice structure, and is very brittle in nature. To avoid damage, the material is drawn in an unprocessed state and wound prior to subjecting the material to a heat treatment cycle that produces the intermetallic Nb₃Sn. This reaction process, which occurs at ~650 °C, adds an additional processing step to the fabrication when compared to NbTi.

The magnetic design is based on a solid low carbon steel mandrel structure into which grooves are machined to accommodate the coils. The result is a single structure that provides all of the magnetic and structural characteristics of a half-undulator. The half-undulator is wound from a single continuous length of wire (0.6-mm diameter) with alternating wire directions in neighboring coil packs (56 turns). Insulation in the form of a glass

braid with a thickness of less than 60 μm will be used to electrically isolate the wire. Two sets of end correction coils are used to cancel dipole fields inside the undulator and to correct for end kicks. The 2nd field integral is zero by choice of a symmetric magnetic configuration.

The Nb₃Sn prototype is shown in Figure 4, including the single-piece undulator core, an end corrector that is decoupled from the main core, and a joint section where the brittle Nb₃Sn conductor is soldered to NbTi cable.

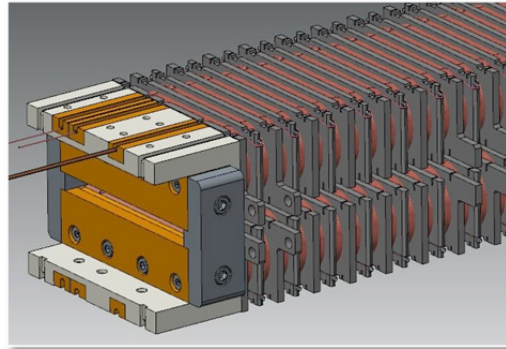


Figure 4: Nb₃Sn prototype undulator magnet design.

MAGNETIC MEASUREMENTS

The APS SCU horizontal magnetic measurement system incorporates Hall probe mapping for determining local field and phase errors, and a stretched-wire rotating coil system for measuring both static and dynamic field integrals and integrated multipole coefficients. The horizontal measurement system incorporates a heated warm-bore Ti tube inside a cold beam chamber. This design allows switching between the Hall probe and the rotating coil measurement system while the SCU is at cryogenic temperatures. The Hall sensor is housed in a small carbon fiber tube and is driven by a 3.5-m long linear stage. The carbon fiber tube slides inside the Ti tube during a field measurement [14]. For integrated field measurements, the integral coil (which is inside the Ti tube) is continuously rotated by two precision rotary stages and uses a lock-in amplifier technique for improved sensitivity and noise rejection [15]. The effective resolution of the Hall probe measurement scan is 0.1 Gauss with five measurement points per millimeter. Repeatability of the measured 1st and 2nd field integrals are ±0.5 G-cm and ±100 G-cm² respectively, well below the LCLS-II HXU FEL tolerances.

Wire-based methods, such as pulsed wire or vibrating wire techniques, can readily be used in small gap devices or where space restrictions make other measurement methods more difficult. For both methods, a wire is stretched along the length of the undulator and current is passed through the wire, generating either a local disturbance (pulsed wire method) or a global wire vibration (vibrating wire method) due to the Lorentz force. For the pulsed wire technique, the shape of the disturbance can be related to the first and second field integrals of the magnetic field (depending on the length of the current pulse), making this an attractive candidate for

field-integral measurements. A pulsed-wire measurement system has been constructed at LBNL and will be applied to the measurement of the superconducting undulators. Significant effort has been placed in the improvement of the pulsed wire method in order to obtain accurate measurements in undulators, especially those with short period lengths. Specifically, algorithms that correct for finite pulse width and dispersive effects in the wire motion have been developed in order to obtain accurate field integral and phase error measurements [11].

MAGNETIC CORRECTIONS

In order to reduce magnetic field errors, much of the focus will be placed on accurate winding methodologies and machining processes. Nevertheless, for long devices, corrections may be necessary for the stringent tolerances on trajectories and phase errors in an FEL. The methods include end corrections, and phase error and trajectory corrections in the periodic section of the undulator. A tuning scheme using YBCO tape-based single-turn coils and superconducting switches will be implemented for corrections in the periodic section of the device. The coils can be activated by using heater switches, which divert the current from a bypass path to individual coils. Since all of the coils are wired in series, the current through all active coils is equivalent. Therefore, the correction is performed with a single variable current source with variable *on/off* single-turn coils which can be activated at desired locations along the device. It can then be used to tune the undulator in-situ while magnetic measurements are performed. Figure 5 shows the concept, including the main tape, the soldered single-turn coil tapes, and the switching heaters. When a heater is *off*, the current bypasses its single-turn coil. When a heater is *on*, a majority of the current (> 95%) passes through that single-turn coil for field correction.

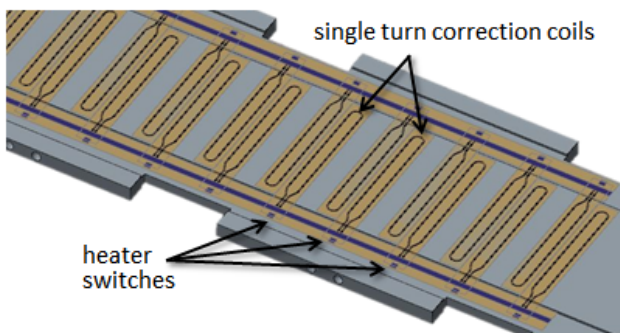


Figure 5: Periodic section field tuner on both sides of chamber.

The single-turn correction coils (0.1 mm thick) will be placed on each side of the vacuum chamber under the undulator poles. The coils will be placed in a pattern that allows for positive and negative kick corrections as well as positive and negative phase error corrections. A switching network and corrector scheme using patterned superconducting (YBCO) tapes and sputtered heaters has been developed at LBNL [9]. A new scheme that uses

resistive joints is being developed for the tuning of the undulator prototypes.

THE CRYOSTATS

Two 4-K *LHe* cryostats are being prepared for the R&D program, with a small tuning cryostat developed at LBNL to allow early testing of field measurement and correction techniques. In addition, a larger 2-m long cryostat, based on the existing design in Ref. [4], is being constructed at ANL. This larger cryostat will be used to do the full SCU testing for each magnet in sequence. The details of each cryostat are described in the two sections below.

The Small Tuning-Cryostat at LBNL

A small cryogen-free cryostat will be used for the field tuning R&D at LBNL. This cryostat can accommodate the full-length (1.5 m) field corrector (Figure 5) and its supporting vacuum chamber. The cold components in the cryostat are cooled with two pulsed tube cryocoolers. A radiation shield is cooled with the first stage of cryocoolers, while the tuner system will be cooled with the second stage of cryocoolers. Current leads with a 100-A capacity will be used to power the tuning system.

The 2-m Test-Cryostat at ANL

The 2-m test cryostat shown in Figure 6 is a copy of the SCU0 cryostat which has been in service in the APS storage ring since January 2013 [16]. Refrigeration at 4.3K is provided by a pair of cryocoolers thermally linked to a 100-liter *LHe* reservoir piped to the magnets. Since the available cooling power exceeds the heat load, the system operates in full recondensation mode with zero helium boil-off. Cold mass, thermal shield, and vacuum vessel geometry are large enough to accommodate both the ANL and LBNL magnet designs, including instrumentation and magnetic measurement systems.



Figure 6: ANL cryostat for testing each of the SCU magnets.

FULL SYSTEM CONCEPT FOR LCLS-II

A concept for a full LCLS-II undulator system is being developed simultaneously with the prototype program. A possible layout is shown in Figure 7, with two 2-m long

SC-undulator sections making up one 5-m cryostat with 0.5-m “cold” magnetic breaks. The system is composed of (up to) 29 cryostats for a full length of (up to) 145 m. Each break includes a cold cavity BPM with $\sim 1 \mu\text{m}$ rms position resolution, a cold quadrupole focusing magnet, steering coils, and a cold adjustable phase shifter. The undulator parameters will be similar to those of Table 1.

System layout could follow the “minimal segmentation” concept used for the SC-linac, with cold cryostat interconnects, common insulating vacuum, and internal cryogenic distribution throughout the undulator string. Segmentation at some level may be desirable from a maintenance or functional standpoint although the packing factor (0.8), heat load, and cryogenic distribution system cost would be adversely impacted. Cooling would likely be provided by a small closed-cycle 4-K cryogenic refrigerator in the several-hundred Watt class, providing both magnet and thermal shield cooling. The refrigerator would be separate and independent from the SC-linac cryoplant for reasons of operational flexibility, differences in cooling requirements, and physical system location.

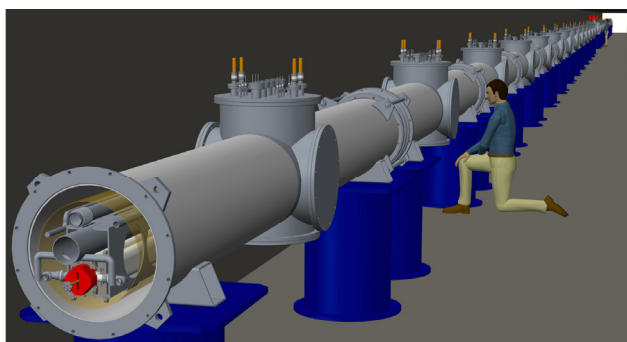


Figure 7: Conceptual SCU system layout for LCLS-II HXU.

DISCUSSION

The performance of the LCLS-II HXR FEL can be greatly improved by choosing superconducting undulators, allowing a much wider photon tuning range, a far longer undulator lifetime, and the possibility of generating terawatt peak power levels from a tapered, self-seeded FEL. Practical development of this technology is the key to making this decision. A baseline LCLS-II design change is possible, but not before completion of the R&D prototypes (July 2015) and a fully developed plan with LCLS-II project impact estimated.

ACKNOWLEDGMENT

Work supported by the Director, Office of Science, of the U.S. Department of Energy under Contract No. DE-AC02-76SF00515, DE-AC02-05CH11231, and DE-AC02-06CH11357.

REFERENCES

- [1] J. Bahrtdt, Y. Ivanyushenkov, “Short Period Undulators for Storage Rings and Free Electron Lasers”, *Journal of Physics, Conf. Series*, **425** (2013), 032001.
- [2] T. Raubenheimer, “The LCLS-II, a New FEL Facility at SLAC”, in *Proc. of 36th Int. Free-Electron Laser Conf.*, Basel, 2014, WEB001.
- [3] P. Emma *et al.*, “The Linear Accelerator Design for the LCLS-II FEL Facility”, in *Proc. of 36th Int. Free-Electron Laser Conf.*, Basel, 2014, THP025.
- [4] Y. Ivanyushenkov *et al.*, “Experience of Operating a Superconducting Undulator at the Advanced Photon Source”, In *Proc. of 2011 Part. Acc. Conf.*, New York, NY, pp. 2053-2055, WEP0049.
- [5] R. Rossmannith *et al.*, “A Year’s Experience with a Superconducting Undulator in the Storage Ring ANKA”, in *Proc. of 2006 EPAC*, Edinburgh, Scotland, pp. 3571-3573, THPLS123.
- [6] B. Podobedov, “Resistive Wall Wakefields in the Extreme Anomalous Skin Effect Regime”, *Phys. Rev. ST - AB*, **12**, 044401, 2009.
- [7] M. Xie, “Design Optimization for an X-Ray Free Electron Laser Driven by SLAC Linac”, in *Proc. of 1995 Part. Acc. Conf.*, Dallas, TX, pp. 183-185, (1995), TPG10.
- [8] J. Amann *et al.*, “Demonstration of Self-seeding in a Hard-X-ray Free-electron Laser”, *Nature Photonics*, **6**, 693-698, 2012.
- [9] D. Arbelaez *et al.*, *IEEE Transactions on Applied Superconductivity*, Vol. **23**, No. 3, June 2013.
- [10] K. Harkay *et al.*, “APS Superconducting Undulator Beam Commissioning Results”, in *Proc. of 2013 Part. Acc. Conf.*, Pasadena, CA, pp. 703-705, WEOAA3.
- [11] D. Arbelaez *et al.*, “A Dispersion and Pulse Width Correction Algorithm for the Pulsed Wire Method”, *NIM A*, Vol. **716**, pp. 62-70.
- [12] D. Dieterich *et al.*, “Fabrication of a Short-Period Nb₃Sn Superconducting Undulator”, *IEEE Trans. on Applied Superconductivity*, Vol. **17**, No. 2, June 2007, pp. 1243-1246.
- [13] Y. Ivanyushenkov *et al.*, “Development of a Planar Superconducting Undulator for the Advanced Photon Source”, *IEEE Trans. on Applied Superconductivity*, Vol. **22**, No. 3, June 2012.
- [14] Y. Ivanyushenkov *et al.*, “Development Status of a Magnetic Measurement System for the APS Superconducting Undulator”, In *Proc. of 2011 Part. Acc. Conf.*, New York, NY, pp. 1286-1288, TUP243.
- [15] C. Doose, M. Kasa, “Magnetic Measurements of the First Superconducting Undulator at the Advanced Photon Source”, in *Proc. of 2013 Part. Acc. Conf.*, Pasadena, CA, pp. 1238-1240, THPBA06.
- [16] J. Fuerst *et al.*, “Cryogenic Performance of a Cryocooler-Cooled Superconducting Undulator”, *Adv. Cryo. Eng.*, *AIP Conf. Proc.*, **1573**, pp. 1527, 2014.